JGR Biogeosciences

RESEARCH ARTICLE
10.1029/2021JG006516

Assessing the Role of Photochemistry in Driving the Composition of Dissolved Organic Matter in Glacier Runoff

Amy D. Holt[1], Anne M. Kellerman[1], Wenbo Li[1], Aron Stubbins[2], Sasha Wagner[3], Amy McKenna[4], Jason Fellman[5], Eran Hood[5], and Robert G. M. Spencer[1]

[1]National High Magnetic Field Laboratory Geochemistry Group and Department of Earth, Ocean, and Atmospheric Science, Florida State University, Tallahassee, FL, USA, [2]Departments of Marine and Environmental Science, Civil and Environmental Engineering, and Chemistry and Chemical Biology, Northeastern University, Boston, MA, USA, [3]Department of Earth and Environmental Sciences, Rensselaer Polytechnic Institute, Troy, NY, USA, [4]National High Magnetic Field Laboratory, Florida State University, Tallahassee, FL, USA, [5]Alaska Coastal Rainforest Center and Program on the Environment, University of Alaska Southeast, Juneau, AK, USA

Abstract Dissolved organic matter (DOM) in glacier runoff is aliphatic-rich, yet studies have proposed that DOM originates mainly from allochthonous, aromatic, and often aged material. Allochthonous organic matter (OM) is exposed to ultraviolet radiation both in atmospheric transport and post-deposition on the glacier surface. Thus, we evaluate photochemistry as a mechanism to account for the compositional disconnect between allochthonous OM sources and glacier runoff DOM composition. Six endmember OM sources (including soils and diesel particulate matter) were leached and photo-irradiated for 28 days in a solar simulator, until >90% of initial chromophoric DOM was removed. Ultrahigh-resolution mass spectrometry was used to compare the molecular composition of endmember leachates pre- and post-irradiation to DOM in supraglacial and bulk runoff from the Greenland Ice Sheet and Juneau Icefield (Alaska), respectively. Photo-irradiation drove molecular level convergence between the initially aromatic-rich leachates and aromatic-poor glacial samples, selectively removing aromatic compounds ($-80 \pm 19\%$ relative abundance) and producing aliphatics ($+75 \pm 35\%$ relative abundance). Molecular level glacier runoff DOM composition was statistically indistinguishable to post-irradiation leachates. Bray-Curtis analysis showed substantial similarity in the molecular formulae present between glacier samples and post-irradiation leachates. Post-irradiation leachates contained $84 \pm 7.4\%$ of the molecular formulae, including $72 \pm 17\%$ of the aliphatic formulae, detected in glacier samples. Our findings suggest that photodegradation, either in transit to or on glacier surfaces, could provide a mechanistic pathway to account for the disconnect between proposed aromatic, aged sources of OM and the aliphatic-rich fingerprint of glacial DOM.

Plain Language Summary Several organic matter (OM) sources have been suggested to contribute to the dissolved organic matter (DOM) composition found in glacier runoff. Often, these sources are aged and aromatic at their origin (e.g., soil and fossil fuel combustion byproducts). Although glacier DOM is old, its composition is aliphatic-rich. Therefore, DOM leached from the proposed sources does not have the same composition as glacier DOM. Given the intense light that DOM is exposed to during atmospheric transport and on glacier surfaces, we suggest that photodegradation could explain the compositional disconnect. We explore this mechanism through a series of laboratory light exposure experiments, where OM sources (e.g., soil and diesel particulate matter) are leached in ultrapure water and their molecular composition assessed before and after light exposure using ultrahigh-resolution analytical techniques. We compare laboratory-generated leachates before and after light exposure to field-collected glacier samples, to determine if observed glacier DOM composition can be created through photodegradation. Initially leachates were dissimilar to glacier DOM composition (i.e., relatively aromatic enriched compared to glacier samples). After photodegradation DOM leachates had a similar molecular fingerprint as glacier DOM. Our results suggest that photochemical degradation of aged, aromatic OM could explain the composition of DOM in glacier runoff.

Key Points:

- Pre-irradiation leachate dissolved organic matter composition (DOM) was aromatic enriched and dissimilar to glacier DOM
- Photo-irradiation drove compositional convergence between leachate DOM composition and glacial samples, by producing aliphatic compounds
- Photochemistry may explain the disconnect between aged, aromatic organic matter and the aged, aliphatic-rich composition of glacier DOM

Supporting Information:

Supporting Information may be found in the online version of this article.

Correspondence to:

A. D. Holt,
adh19d@my.fsu.edu

Citation:

Holt, A. D., Kellerman, A. M., Li, W., Stubbins, A., Wagner, S., McKenna, A., et al. (2021). Assessing the role of photochemistry in driving the composition of dissolved organic matter in glacier runoff. *Journal of Geophysical Research: Biogeosciences*, *126*, e2021JG006516. https://doi.org/10.1029/2021JG006516

Received 30 JUN 2021
Accepted 4 NOV 2021

1. Introduction

Glaciers export ancient, bioavailable dissolved organic carbon (DOC) to downstream ecosystems (DOC age 750–10,800 years, Bhatia et al., 2013; Fellman, Hood, Raymond, Hudson, et al., 2015; Hood et al., 2009; Lawson, Bhatia, et al., 2014; Lawson, Wadham, et al., 2014; Singer et al., 2012; Spencer, Guo, et al., 2014; Stubbins,

Hood, et al., 2012). The composition of glacier dissolved organic matter (DOM) underpins this high DOC bioavailability, due to the high relative abundance (RA) of aliphatic and peptide-like molecular formulae (Antony et al., 2017; Hemingway et al., 2019; Lawson, Bhatia, et al., 2014; Stubbins, Hood, et al., 2012). Given the high bioavailability of glacier DOC and that glaciers and ice sheets store an estimated 6 Pg of organic carbon globally, with an annual DOC flux of 1.04 ± 0.18 Tg C yr^{-1} to the ocean (Hood et al., 2015), understanding the main sources and cycling of DOM exported from glacier ecosystems has implications for the atmospheric CO_2 pool.

A range of sources have been proposed to explain the composition, age and bioavailability of glacier DOM. To date, no source explains all attributes of glacier DOM, particularly why the bioavailability of glacier DOC increases with radiocarbon (^{14}C) age (Singer et al., 2012; Spencer, Guo, et al., 2014; Stubbins, Hood, et al., 2012), resulting in a disconnect between the documented sources and the DOM composition found in supra- and subglacial runoff. Proposed organic matter (OM) sources include autochthonous microbial production on or beneath the glacier, which generates bioavailable DOM (i.e., aliphatic and peptide-like compounds, Antony et al., 2014; Musilova et al., 2017; Smith et al., 2017; Wadham et al., 2004). Hence, autotrophy could explain the composition and bioavailability of glacial DOM (Bhatia et al., 2010; Lawson, Bhatia, et al., 2014; Musilova et al., 2017; Zhou, Zhou, Hu, et al., 2019); yet it remains unclear how this freshly produced DOC can be highly ^{14}C deplete, particularly when dissolved inorganic carbon has been shown to be comparatively contemporary in supraglacial and subglacial runoff of the Greenland Ice Sheet (Andrews et al., 2018). Microbial metabolism of subglacial palaeo OM (i.e., soils and vegetation overridden during ice advance) may also provide ancient bioavailable DOM compounds to glacier outflows. However, little is known about the metabolic potential beneath glaciers and ice sheets (Stibal, Hasan, et al., 2012), including the reactivity of the substrate and the capacity of subglacial microbes to utilize this OM.

Allochthonous sources of OM to glacier surfaces include aeolian deposition of locally sourced soil and vascular plant-derived OM (Barker et al., 2009; Bhatia et al., 2010; Hood et al., 2009; Singer et al., 2012), and distantly sourced aerosols, including organic products from biogenic and fossil fuel combustion (Fellman, Hood, Raymond, Stubbins, & Spencer, 2015; Li et al., 2018; Price et al., 2009; Spencer, Guo, et al., 2014; Spencer, Vermilyea, et al., 2014; Stubbins, Hood, et al., 2012). These sources vary in their apparent ^{14}C age, for example fossil fuel carbon is ^{14}C dead, whereas recently deglaciated soil OM has been shown to be thousands of years old (Bardgett et al., 2007). These sources could explain the age of glacial DOC (Singer et al., 2012; Spencer, Guo, et al., 2014; Stubbins, Hood, et al., 2012). However, at their point of origin, proposed allochthonous OM sources have high aromaticity (Chen & Jaffé, 2014; Fellman et al., 2013; Hansen et al., 2016; Li et al., 2018; Masiello, 2004). Therefore, it remains to be determined how these sources when deposited on the glacier surface contribute to the highly bioavailable, aliphatic-rich DOM widely observed in glacier runoff.

Photochemical transformations are known to breakdown aromatic DOM, such as condensed aromatics and lignin phenols (Spencer et al., 2009; Stubbins et al., 2010), in the atmosphere and in aquatic environments (Bertilsson & Tranvik, 2000; Gonsior et al., 2009; Laurion & Mladenov, 2013; Stubbins & Dittmar, 2015; Stubbins et al., 2008). The role of photochemistry in altering the composition of OM in glacier ecosystems (including in aqueous solution and solid ice phase) has received recent research attention, particularly with regard to the persistence, storage and release of organic anthropogenic pollutants from glaciers (e.g., Ferrario et al., 2017; Franzetti et al., 2016; Grannas et al., 2004, 2007, 2013; Herbert et al., 2006; Kahan & Donaldson, 2007; Klán et al., 2003; Ram & Anastasio, 2009). Despite this research, photochemistry has not been directly linked to the aged, aliphatic signature of DOM in glacier runoff, having just been considered during in situ incubations and snowpack analysis (e.g., Antony et al., 2014, 2018). In both these assessments, allochthonous DOM sources have likely already been modified from their composition at the point of origin, first during atmospheric transport and then post-deposition on the glacier surface (George et al., 2015; Singer et al., 2012). Without considering the compositional transformations that allochthonous OM sources undergo during atmospheric transport and within glacier ecosystems, there may be misassignment of the sources of OM that explains the molecular signature of glacier DOM. Thus, evaluating the potential photochemical transformations that allochthonous OM sources may undergo, both during atmospheric transport and within glacier ecosystems, could help to identify the sources of OM responsible for the unique, ancient aliphatic-rich molecular signature of DOM in glacier runoff.

In this study, we examined how photochemical degradation alters the composition of DOM from six postulated allochthonous endmember sources of OM to supraglacial environments. Our aim was purely to determine if simulated photodegradation of allochthonous OM sources can reproduce the molecular signature of DOM in

supra- and subglacial runoff (from herein collectively termed glacier runoff). We did not attempt to assess rates of photodegradation or determine the site or phase of this processes in the environment. Ultrahigh-resolution electrospray ionization Fourier transform ion cyclotron resonance mass spectrometry (FT-ICR MS) was used to analyze the shifts in molecular level composition of DOM pre- and post-irradiation. The DOM composition of endmembers pre- and post-irradiation were compared to supraglacial and bulk runoff samples from the Greenland Ice Sheet and Juneau Icefield (Alaska), respectively. We hypothesized that simulated photodegradation can transform the DOM chemistries of a diverse suite of allochthonous, aromatic-rich laboratory-generated endmember leachates towards the aliphatic-rich chemistry of DOM found in glacier runoff.

2. Materials and Methods

2.1. Endmember Source and Sample Collection

Six endmembers were chosen to reflect the range of allochthonous OM sources postulated to contribute to glacier surface DOM (Singer et al., 2012; Spencer, Guo, et al., 2014; Stibal, Šabacká, & Žárský, 2012; Stubbins, Hood, et al., 2012). Two charcoal samples, rice and wood char (RC and WC, respectively) were selected as sources of burnt biomass (sourced from the University of Zurich, Switzerland), with details of formation and characterization in Hammes et al. (2006). Two anthropogenic endmembers were chosen, urban dust (UD) and diesel particulate matter (DPM; ^{14}C dead). Both are standard reference materials from the National Institute of Standards and Technology, USA (1694b and 2975, respectively). Lastly, two local endmember sources to glacier surfaces, proglacial vegetated and recently deglaciated (barren) soil (VS and DGS, respectively), from the Mendenhall Glacier catchment, southeast Alaska (58.43°N, 134.55°W) were collected.

For comparison purposes, glacier DOM was sampled as bulk runoff at the outflow of Mendenhall and Herbert Glaciers (58.44°N, 134.54°W; 58.54°N, 134.68°W, respectively), southeast Alaska and as supraglacial runoff (two samples: pooled meltwater and a supraglacial stream) from Russell Glacier, southwest Greenland Ice Sheet (67.14°N, 49.93°W). All glacial samples were filtered immediately at the field sites through 0.7 μm precombusted (450°C, 5 hr) GF/F filters and stored in prerinsed, acid-washed (10% HCl v/v for 48 hr) polycarbonate bottles. All solid endmembers and glacial samples were kept frozen at −20°C, in the dark, until further processing.

2.2. Formation of Leachates

Solid endmembers were thawed in the dark at 20°C. Soil samples were dried at 50°C for 48 hr. Each dried solid endmember (0.2 g organic carbon) was weighed directly into a pre-rinsed (three times with ultrapure water; UPW), precombusted (550°C), acid-washed (10% HCl v/v for 48 hr) conical flask and 200 mL of UPW added. The mixture was capped, placed on a shaker table, and agitated for 72 hr at 20°C, in the dark. Subsequently, each mixture was filtered through a 0.22 μm Sterivex™ filter into a pre-rinsed, acid-washed (10% HCl v/v for 48 hr) opaque Nalgene® bottle and frozen (− 20°C) until further processing.

2.3. Full-Spectrum Photochemical Irradiation Experiments

The leachates were thawed, mixed and 100 mL of each leachate transferred into 100 mL acid washed (10% HCl v/v 48 hr) and precombusted (550°C, 5 hr) quartz round bottom flasks. The DGS leachate was diluted with UPW (1:9 v/v) prior to sample irradiation to reduce self-shading effects during the experiment. Samples were stoppered, placed inside a solar simulator (Atlas Suntest XLS+), and irradiated for 28 days. The Suntest was equipped with a 1.5 kW xenon lamp and a daylight filter, resulting in simulated sunlight with intensity and spectral quality like that of natural sunlight and specifically designed to match that of CIE 85 reference global solar radiation (CIE, 1989).

2.4. DOC and CDOM Analyses

For each leachate, chromophoric DOM (CDOM) data were collected on days 0, 2, 4, 7, 10, and 28 during the irradiation experiment. Absorbance spectra (200–800 nm) were collected using a Horiba Aqualog-UV-800-C spectrophotometer and a quartz cuvette with a 1 cm path length. Sample spectra were corrected using UPW blank spectra. If the optical density (A) at 250 nm of any sample exceeded a value of 2 (dimensionless), the sample was

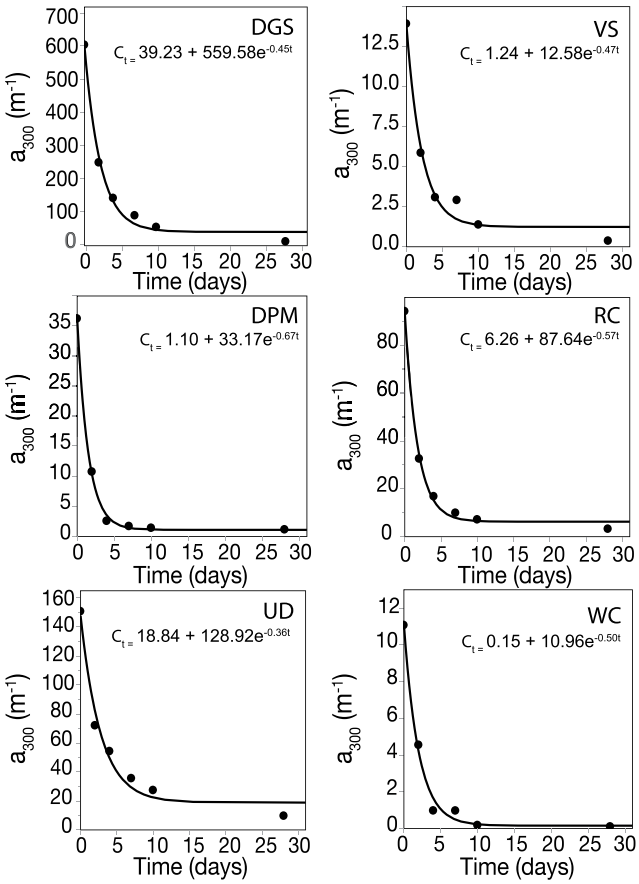

Figure 1. Three-parameter exponential decay model of chromophoric dissolved organic matter (CDOM) for all endmembers through the 28-day photodegradation experiment. Sample ID displayed on each panel (see Section 2.1 for details of abbreviations). Three parameter model expressed as $C_t = C_x + Z_0e^{-kt}$, where C_t is the modeled absorbance at 300 nm at a time (t) point, C_x is the photo-unreactive component, Z_0 is an adjustable parameter that represent the photoreactive component at time 0, k is the rate of decay (Spencer et al., 2009).

diluted with UPW and reanalyzed. Per sample, the optical density at 300 nm was converted to Naperian absorbance coefficients (a_{300}; m^{-1}) to assess sample photobleaching (Hu et al., 2002). CDOM light absorbance at 300 nm was tracked throughout the irradiations to ensure all samples were extensively and comparatively photobleached (>90% of initial CDOM removed) and reached the asymptote of exponential decay (Figure 1). DOC concentrations were measured for all glacial samples, and endmember leachates pre- and post-irradiation, using a Shimadzu TOC-L_{CPH} high-temperature catalytic oxidation total organic carbon analyzer. DOC concentration was calculated with standard methodology using a six-point standard curve on the average of three to seven injections, with a coefficient of variance <2% (Mann et al., 2012).

2.5. FT-ICR MS Analysis

FT-ICR MS analysis was carried out on all glacial samples and source endmember leachates pre- and post-irradiation. All samples were acidified to pH 2 using reagent grade HCl, then extracted via solid phase extraction, onto pre-cleaned 100 mg Bond Elut PPL cartridges (Agilent Technologies; Dittmar et al., 2008). The volume of each sample extracted was adjusted dependent on the DOC concentration of the sample, with a target DOC loading of 40 μg C mL^{-1}. High DOC concentration low volume samples were diluted before extraction, to ensure enough volume to allow distribution of DOM across the PPL resin. Once the sample was passed over the PPL, the cartridges were rinsed twice with 0.01 M HCl, to remove any inorganics (Spencer, Guo, et al., 2014). Then, the columns were dried with a flow of carbon free nitrogen gas. DOM was eluted from each cartridge with 1 mL of HPLC-grade methanol into 2 mL precleaned (10% HCl v/v 48 hr) and combusted (550°C, 5 hr) amber glass vial. Samples were refrigerated (4°C) until analysis.

The eluted samples were analyzed using electrospray ionization in negative mode on the 21 tesla FT-ICR MS at the National High Magnetic Field Laboratory (NHMFL), Florida, USA. One hundred scans were accumulated for the mass spectra. Collected data were internally calibrated with a "walking" calibration equation (Savory et al., 2011). Molecular formulae were assigned to peaks with greater than six times the baseline signal to noise, using PetroOrg software. The RA of formulae containing only carbon, hydrogen and oxygen (CHO-only), and these elements with the addition of nitrogen and/or sulfur (CHON, CHOS and CHONS) was calculated to determine the RA of different heteroatom classes (i.e., the percent contribution of all peaks belonging to a class as a fraction of the total signal off all assigned peaks in a sample). The modified aromaticity index (AI_{mod}) and nominal oxidation state of carbon (NOSC) was calculated for each formula (Koch & Dittmar, 2006, 2016; Riedel et al., 2012). Formulae with AI_{mod} values of 0.5–0.67 and >0.67 were classed as polyphenolic and condensed aromatics, respectively (Koch & Dittmar, 2006). Other compound classes were highly unsaturated and phenolic (HUP), AI_{mod} of <0.5 and H/C < 1.5; aliphatic, H/C ≥ 1.5–2.0, O/C ≤ 0.9 and $N = 0$; peptide-like, H/C ≥ 1.5–2, O/C ≤ 0.9 and $N > 0$; and sugar-like, H/C ≥ 1.5–2 and O/C > 0.9 (Koch & Dittmar, 2006; Spencer, Guo, et al., 2014; Zito et al., 2019). This classification is based on stoichiometric similarity, not necessarily compound structure since formulae within each class may consist of multiple isomers.

Comparative analysis of the FT-ICR MS mass spectra for each endmember was conducted to categorize molecular formulae into different photodegradation classes. Formulae that were only present pre-irradiation and post-irradiation were categorized as photolabile and photoproduced, respectively, and those which persisted throughout were categorized as photoresistant. Photoresistant fractions may change in RA pre- and post-irradiation, thus these molecular formulae are not necessarily stable. Similarly, they are comprised of an unknown number of isomers, and therefore a formula may differ in chemical structure (or proportions thereof) pre- and post-irradiation. In order to understand shifts in DOM composition that are common across endmember sources, we compiled

molecular formulae of the same photodegradation class that were present across four or more endmembers. Similarly, molecular formulae that were present across all glacial samples were collated and used to form a core glacier signature, enabling a comparison of endmembers to molecular formulae, typically found in glacial runoff DOM. Furthermore, in order to understand the similarity between endmember leachates post-irradiation and the glacial samples, we compiled common molecular formulae across four or more post-irradiation endmember leachates that were also present in the core glacier signature. Individual van Krevelen diagrams of glacial samples and endmember leachates are presented in Figure 2, and formulae categorized as photolabile, photoproduced and photoresistant for each endmember are shown in Figure S1.

2.6. Statistical Methods

All statistical analysis was conducted using R (Version 1.1.463; R Core Team, 2020). A non-parametric Wilcox signed-rank test was used to analyze the difference in the mean RA weighted compound classes, mass, NOSC, as well as the DOC concentrations among all endmembers pre- and post-irradiation. This paired test was preferred since intrinsic compositional differences initially present between endmembers were taken into account. Using the stated metrics, endmembers pre- and post-irradiation were compared to glacier samples, using a nonparametric Kruskal-Wallis test. This analysis was chosen since sample groups are independent and even when transformed the data did not follow a normal distribution. Principal component (PC) analysis was conducted (using the FactoMine R package; Lê et al., 2008) in order to understand whether, at the molecular level, the composition of post-irradiated leachates converged toward glacial samples. PC analysis variables included the number of assigned molecular formulae, and RA weighted compound classes, AI_{mod}, mass and NOSC. Variables were standardized to unit variance, to ensure those on different measurement scales were comparable and hence did not skew the PC analysis output. All endmembers (pre- and post-irradiation) and glacial samples were included individually in this analysis. Bray-Curtis dissimilarity analysis was performed using the Ecodist R package (Goslee & Urban, 2007), in order to assess whether the molecular diversity of samples converged post-irradiation with individual glacier samples and the core glacier signature. Analysis was performed based on presence/absence of molecular formulae. The percentage overlap of common formulae between four or more post-irradiation leachates and the core glacier signature, as well as each individual endmember post-irradiation and the core glacier signature was also determined to provide additional measures of similarity.

3. Results and Discussion

3.1. Glacier DOM

The DOC concentrations of glacial samples (0.22 ± 0.15 mg C L^{-1}; Table S1, Figure 3) were comparable with those reported previously for mountain glacier outflows (0.4 ± 0.1 mg C L^{-1}, $n = 55$) as well as in supraglacial and bulk runoff from the Greenland Ice Sheet (0.2 ± 0.2 mg C L^{-1}, $n = 52$ and 0.3 ± 0.3 mg C L^{-1}, $n = 47$, respectively; Holland et al., 2019; Hood et al., 2015; Kellerman et al., 2020; Lawson, Wadham, et al., 2014; Musilova et al., 2017). All glacial samples were enriched in aliphatic and peptide-like formulae (combined $34 \pm 13\%$ RA), with a small contribution of condensed aromatic and polyphenolic compounds (combined $4.7 \pm 1.7\%$ RA; Table 1, Figures 2–4). Glacier DOM is similar in molecular composition to water soluble organic matter (WSOM) observed from aerosols across a variety of air masses and DOM observed in precipitation (snowfall and rainfall) over mountainous glacier regions (Fellman, Hood, Raymond, Stubbins, & Spencer, 2015; Gurganus et al., 2015; Li et al., 2018; Wozniak et al., 2014). Typically, aerosol WSOM has low aromaticity (AI_{mod} 0.09–0.18), is dominated by compounds with high H/C ratios (1.4–1.7, i.e., large aliphatic contribution) and has some fraction of aged material (Gurganus et al., 2015; Kirillova et al., 2013; Li et al., 2018; Wozniak et al., 2014); therefore, WSOM chemistry is similar to the glacier samples analyzed here (AI_{mod} 0.15–0.21 and H/C ratio 1.2–1.4; Table 1). The aliphatic-enriched properties of our glacial samples are reflected in the core glacier signature, which represent molecular formulae present in all glacial samples examined in this study (Figure 5a). This composition is comparable to DOM observed across mountain glaciers and ice sheets world-wide (Behnke et al., 2020; Bhatia et al., 2010; Hemingway et al., 2019; Singer et al., 2012; Spencer, Guo, et al., 2014; Stubbins, Hood, et al., 2012; Zhou, Zhou, He, et al., 2019) and distinct in comparison to most riverine systems, which are typically dominated by aromatic signatures due to direct inputs from allochthonous soil and plant-derived OM (Behnke et al., 2021; Kellerman et al., 2021; Stubbins et al., 2010).

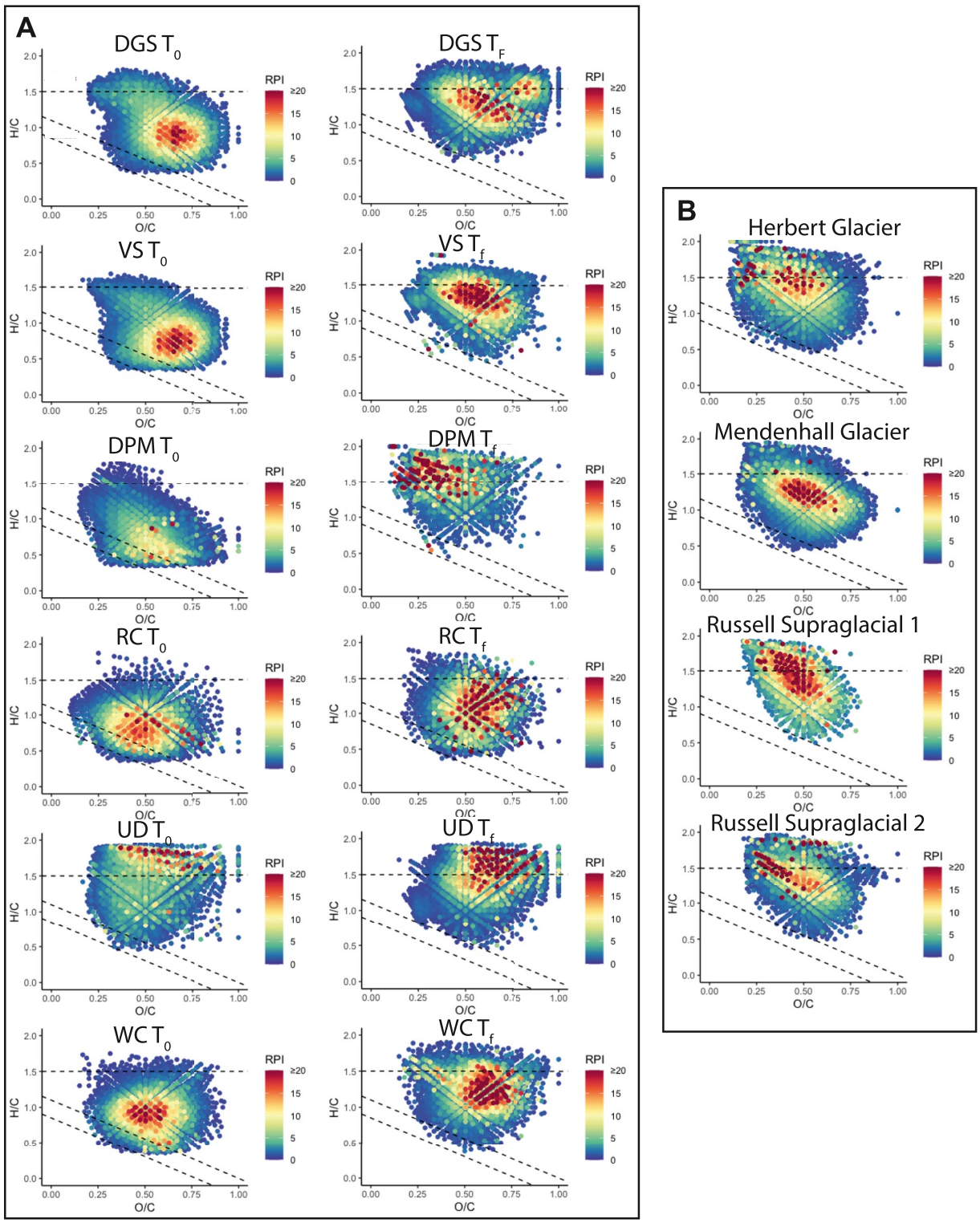

Figure 2. (a) van Krevelen plots of the distribution of dissolved organic matter (DOM) in endmember samples pre- (T_0) and post-irradiation (T_f). (b) Glacier samples for comparison. See titles of each panel for sample ID. Shading represents the relative peak intensity (RPI) of each molecular formula (i.e., the intensity of an individual peak to the total intensity of all peaks assigned in the sample, scaled to 10,000).

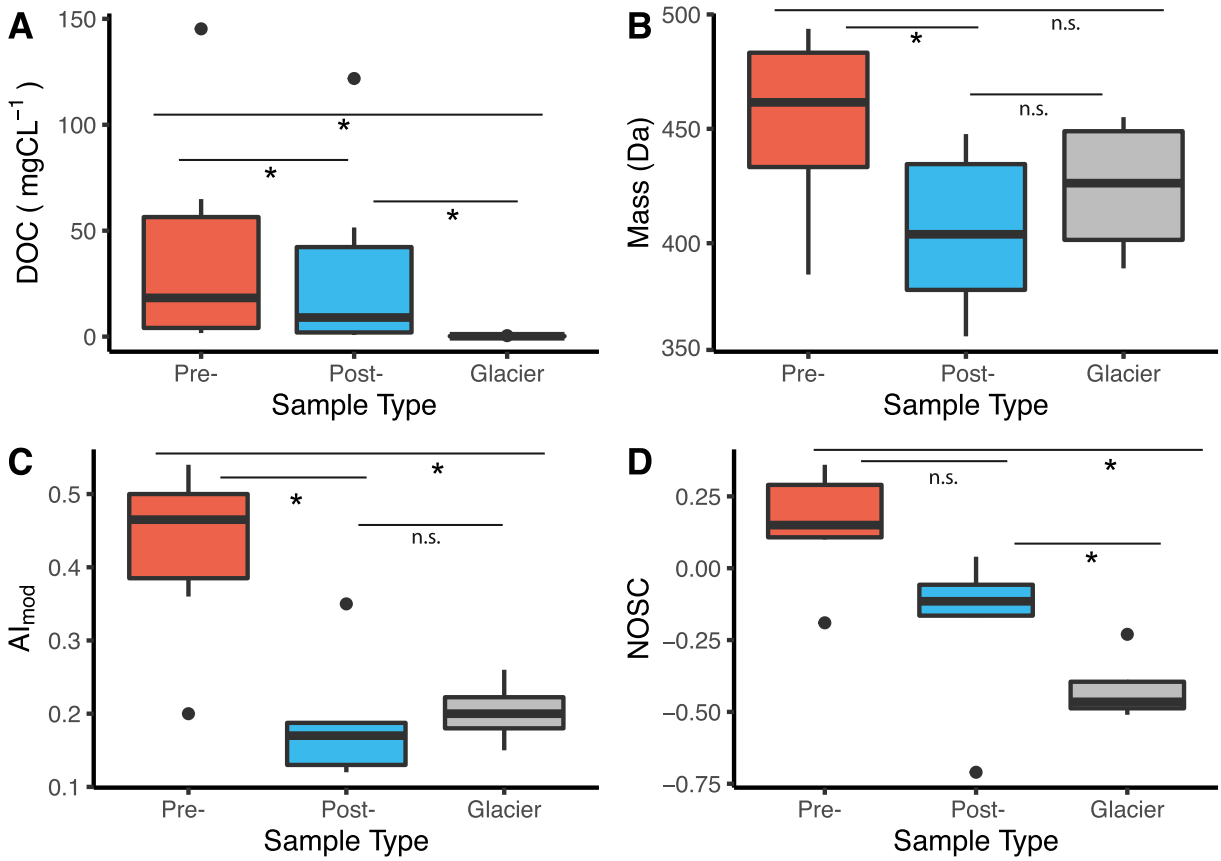

Figure 3. Median (a) dissolved organic carbon (DOC) concentration, and relative abundance (RA) weighted (b) mass, (c) AI_{mod} and (d) nominal oxidation state of carbon (NOSC) across all endmembers pre- and post-irradiation, compared to glacier samples. Horizontal lines indicate significance tests between groups, asterisk denoting significant difference (p-value < 0.05) and "n.s.," referring to no significant difference.

3.2. Molecular Properties of DOM From Leached Endmembers

Leachate DOC concentrations were variable between endmembers (DOC ranged from 1.68 to 145.28 mg C L^{-1}; Table S1), reflecting differences in the leachable fraction of organic carbon between endmember sources. Across endmembers, the DOM composition of pre-irradiation leachates was variable. Both soil leachates (DGS and VS) were dominated by HUP compounds (73.00% and 54.74% RA, respectively) and were enriched in aromatic and polyphenolic compounds (combined 21.06% and 43.61% RA for DGS and VS, respectively; Table 1, Figure 2). DGS had less condensed aromatic and polyphenolic compounds, and higher aliphatic contributions than VS (5.94 compared to 1.66% RA for VS; Table 1). This may be due to relatively greater inputs of microbial OM in baren, recently deglaciated soil compared to soils with established vegetation, since soil microbes have been shown to be important in setting the biogeochemical conditions needed for vegetation to establish following glacier recession (Bardgett et al., 2007; Milner et al., 2007). Alternatively, aliphatic, possibly microbial-derived, DOM inputs may be observed in DGS leachates because they are not overprinted by aromatic DOM derived from vegetation or soil.

The two burnt biomass endmembers (RC and WC) as well as DPM all represent sources dominated by combustion byproducts and thus are enriched in condensed aromatics and polyphenolics, particularly DPM (combined 60.08% RA compared to 53.62% and 38.27% RA for RC and WC, respectively; Table 1, Figure 2). The RA weighted H/C ratios for RC and WC leachates (0.85 and 0.89, respectively) were higher than that reported for the solid endmembers based on molar ratios (H/C 0.7; Hammes et al., 2006). Differences in the DOM aromaticity between RC, WC and DPM leachates are likely a function of parent material (e.g., vegetation species and exposure to biodegradation), temperature of combustion where higher temperatures lead to greater aromaticity (i.e., lower temperature of formation for chars vs. DPM) or the solubility of different condensed aromatic structures present in the solid endmember (Bird et al., 2015; Hammes et al., 2006; Wagner et al., 2017; Wozniak et al., 2020).

Journal of Geophysical Research: Biogeosciences
10.1029/2021JG006516

Table 1

The Number of Molecular Formulae Identified by Fourier Transform Ion Cyclotron Resonance Mass Spectrometry (FT-ICR MS), the Percent Relative Abundance (RA) of Molecular Formulae Assigned to Each Compound Class, Together With Their Average Molecular Weight, Nominal Oxidation State Of Carbon (NOSC) and AI_{mod} for all Endmembers (Pre- and Post-irradiation) and Glacier Samples

	Pre-irradiation						Post-irradiation						Glacier			
	DGS	VS	RC	WC	DPM	UD	DGS	VS	RC	WC	DPM	UD	Herbert outflow	Mendenhall outflow	Russell supraglacial 1	Russell supraglacial 2
Assigned formulae (#)	4154	3630	4805	3392	7279	5257	5218	3304	3927	3035	2752	5095	4768	4493	3994	1522
Mean mass (Da)	485.6	493.7	428.8	476.3	446.8	386.3	436.8	427.9	379.9	447.7	359.3	379.5	389.0	446.9	455.1	405.6
NOSC	0.17	0.33	0.10	0.13	0.36	−0.19	−0.08	−0.17	0.04	−0.15	−0.71	−0.05	−0.45	−0.23	−0.48	−0.51
AI_{mod}	0.36	0.47	0.51	0.46	0.54	0.20	0.16	0.18	0.35	0.19	0.12	0.12	0.21	0.26	0.15	0.19
Condensed aromatic (% RA)	4.28	12.37	12.91	9.33	27.41	1.92	0.46	1.20	5.58	0.90	0.66	0.85	0.91	0.90	0.45	0.66
Polyphenolic (% RA)	16.78	31.24	40.71	28.94	32.67	7.54	1.93	2.26	14.64	3.58	0.95	2.19	4.31	5.73	2.06	3.69
Highly unsaturated and phenolic (% RA)	73.00	54.74	45.89	60.78	39.05	54.14	70.37	75.21	74.43	73.25	29.99	55.26	60.55	78.24	52.92	53.96
Aliphatic (% RA)	5.94	1.66	0.49	0.95	0.87	31.91	20.88	14.44	4.82	22.10	39.71	34.14	28.37	12.55	40.60	41.69
Peptide-like (% RA)	0.00	0.00	0.01	0.00	0.00	4.01	5.51	6.87	0.53	0.04	28.69	6.14	5.86	2.59	3.94	0.00
Sugar-like (% RA)	0.00	0.00	0.00	0.00	0.00	0.48	0.85	0.02	0.00	0.12	0.01	1.41	0.00	0.00	0.04	0.00
CHO-only (% RA)	93.99	92.18	85.95	100.00	43.61	31.20	76.88	73.10	80.18	92.37	51.57	29.46	74.45	84.82	50.82	94.74
CHON-only (% RA)	6.01	7.82	14.05	0.00	48.41	20.75	18.00	20.78	19.58	0.17	31.59	22.56	13.31	12.53	4.08	0.00
CHONS-only (% RA)	0.00	0.00	0.00	0.00	1.21	5.21	0.13	0.00	0.00	0.00	0.63	6.66	0.00	0.00	2.03	0.00
CHOS-only (% RA)	0.00	0.00	0.00	0.00	6.78	42.84	4.99	6.12	0.24	7.46	16.20	41.33	12.24	2.65	43.07	5.26

Note. Sample IDs are abbreviated and detailed within Section 2.1 of the Materials and Methods.

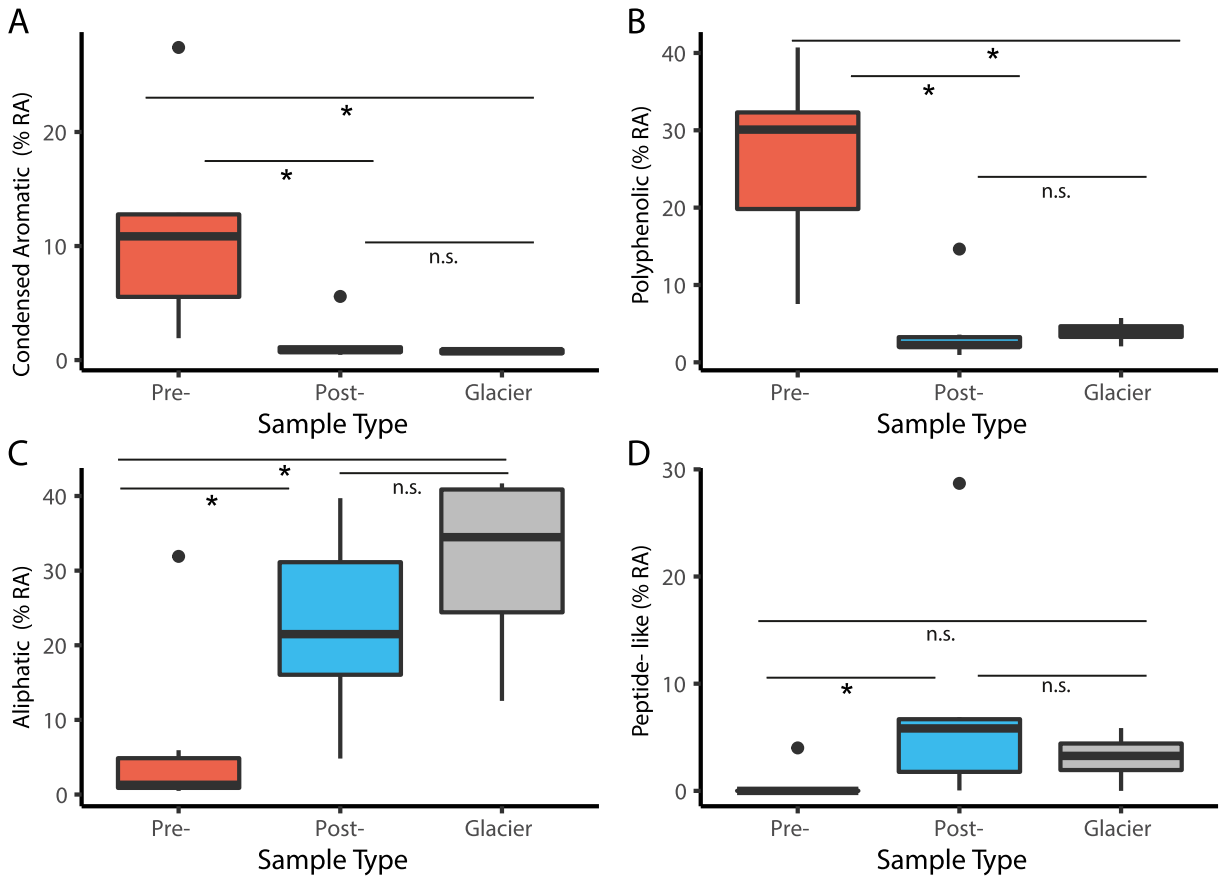

Figure 4. Median relative abundance (RA) of (a) condensed aromatic, (b) polyphenolic, (c) aliphatic and (d) peptide-like compounds across all endmembers pre- and post-irradiation, compared to glacier samples. Horizontal lines indicate significance tests between groups, asterisk denoting significant difference (p-value < 0.05) and "n.s.," referring to no significant difference.

Compared to other pre-irradiation leachates the initial DOM composition of UD was distinctly different, being typically smaller in mass (386.3 Da, mean of pre-irradiation leachates 452.9 ± 40.8 Da), enriched in aliphatic and peptide-like compounds (combined 35.92% RA, mean 7.64 ± 14.0% RA), and low in aromaticity (0.20 AI_{mod}, mean 0.43 ± 0.13; condensed aromatics and polyphenolics combined 9.46% RA, mean 37.7 ± 19.3% RA; Table 1). The molecular composition of UD was also enriched in heteroatom containing formulae, especially CHOS-only compounds compared to other leachates (42.84% RA, mean 8.27 ± 17.2% RA). In urban areas, WSOM in precipitation often has low aromaticity, and is dominated by sulfur containing and aliphatic DOM, which may indicate long-range transport of atmospheric aerosols, including fossil fuel combustion byproducts that have already been photochemically altered during transit (Li et al., 2018, 2020; Mazzoleni et al., 2012; Wozniak et al., 2008).

Despite intrinsic differences in chemical composition between endmember leachates, when all leachates were taken together pre-irradiation DOM composition was compositionally dissimilar to glacier DOM composition (Figures 2–4) and atmospherically derived DOM (i.e., WSOM from atmospheric aerosols and DOM in precipitation; Bhatia et al., 2010; Fellman, Hood, Raymond, Stubbins, & Spencer, 2015; Gurganus et al., 2015; Li et al., 2018; Singer et al., 2012; Spencer, Guo, et al., 2014; Stubbins, Hood, et al., 2012; Wozniak et al., 2014; Zhou, Zhou, He, et al., 2019). Pre-irradiation leachate DOM was typically larger in RA weighted mean mass (453 ± 40.8 Da), contained greater proportions of oxidized carbon (NOSC 0.15 ± 0.20), and was highly aromatic compared to glacier samples (AI_{mod} 0.42 ± 0.13, with a combined RA of condensed aromatic and polyphenolic compounds of 38 ± 19%; Table 1, Figures 3 and 4). Correspondingly, pre-irradiation leachates had a low RA of aliphatic and peptide-like formulae (combined 7.6 ± 14% RA; Table 1). The initial composition of leachates was relatively similar to blackwater riverine DOM draining vegetated watersheds, which are dominated by direct inputs of aromatic vascular plant-derived OM (Behnke et al., 2021; Kurek et al., 2020; Spencer et al., 2015; Stubbins

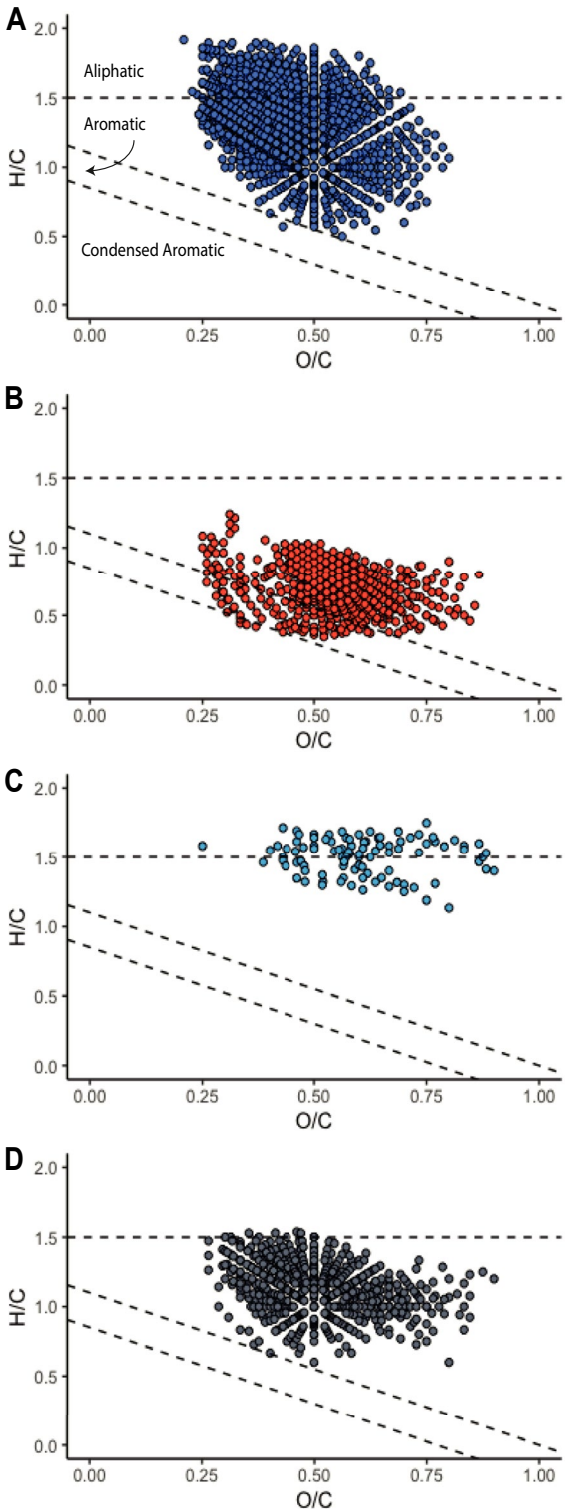

Figure 5. van Krevelen diagrams showing (a) a composite of the common molecular formulae across all glacial samples (core glacier signature), together with common molecular formulae across four or more endmember leachates, separated by photodegradation class: (b) photolabile, (c) photoproduced and (d) photoresistant. Note the similarity in the area occupied in van Krevelen space between combined photoproduced (c) and photoresistant (d) fractions with the core glacier signature (a).

et al., 2010) and thus typically have a high RA of condensed aromatics and polyphenolic compounds and a low RA of aliphatic and peptide-like formulae (Fellman et al., 2014; Seidel et al., 2015; Sleighter & Hatcher, 2008; Stubbins et al., 2010; Stubbins, Hood, et al., 2012). The dissimilar DOM composition between pre-irradiation leachates and glacial samples, as well as atmospherically derived DOM, indicates transformation processes that occur during atmospheric transport or on the glacier surface may be important in altering a significant portion of allochthonous DOM to reflect that observed in supraglacial and bulk runoff.

3.3. Photodegradation Impacts on Endmember Leachates

Photodegradation of all endmember leachates decreased the CDOM absorbance coefficient (a_{300} m^{-1}) and DOC concentrations throughout the 28-day irradiation experiments (Table S1, Figures 1 and 3a). CDOM decline followed a three parameter exponential decay model, and all leachates reached the asymptote of decay (where >90% of initial CDOM was lost) after 28 days of irradiation, signifying minimal change in DOM composition would be observed with continued photo-irradiation (Figure 1). Total DOC loss after 28 days of irradiation varied greatly among endmembers, from 2.1% for WC to 86% for DPM (Table S1, Figure 1a). The loss of DOC following photodegradation can be highly variable for natural waters, as well as biomass and soil leachates (ranging from 0%–90% DOC loss; Chen & Jaffé, 2014; Hansen et al., 2016; Spencer et al., 2009; Stubbins & Dittmar, 2015; Stubbins, Niggemann, et al., 2012). The range of DOC loss observed here is encompassed by those previously reported in the literature and its breadth represents intrinsic differences in the size of the photolabile DOC pool between endmembers.

After photochemical irradiation the aromaticity of endmember leachates was significantly reduced, as shown by the decline in AI_{mod}, and the RA of condensed aromatic and polyphenolic compounds (combined −83 ± 14% RA; Table 1 and Table S2, Figures 2–4). This occurred concomitantly with a significant decline in RA weighted mean molecular mass and an increased RA of aliphatic and peptide-like formulae (combined +78 ± 34% RA; Table 1 and Table S2, Figures 2–4). The NOSC declined in the majority of endmember leachates post-irradiation (Table 1, Figure 2d), however the change was insignificant for all leachates taken together (mean NOSC pre- and post-irradiation 0.15 and −0.19, respectively, p-value 0.09; Table S2, Figure 2d). This is likely due to UD where the NOSC increased following photodegradation (Table 1, see Section 3.4 for further discussion of UD composition). After irradiation, DOM compounds typically contained less oxidized carbon, as shown by both the decline in NOSC in most endmembers and the generally lower RA of CHO-only molecular formulae (Table 1). These changes in DOM composition post-irradiation are consistent with the patterns observed with photodegradation in previous studies of aquatic environments (Antony et al., 2018; Gomez-Saez et al., 2017; Gonsior et al., 2009; Helms et al., 2008; Laurion & Mladenov, 2013; Stubbins & Dittmar, 2015; Stubbins et al., 2010). Photodegradation typically breaks down higher mass, aromatic DOM and produces DOM that is smaller in mass, less aromatic and has a lower NOSC.

Isolating common photolabile molecular formulae (i.e., molecular formulae that are only present pre-irradiation) across multiple endmembers leachates showed that the compounds removed by photodegradation were aromatic or typically had low H/C ratios (mean H/C 0.70 ± 0.17; Figure 5b). Whereas

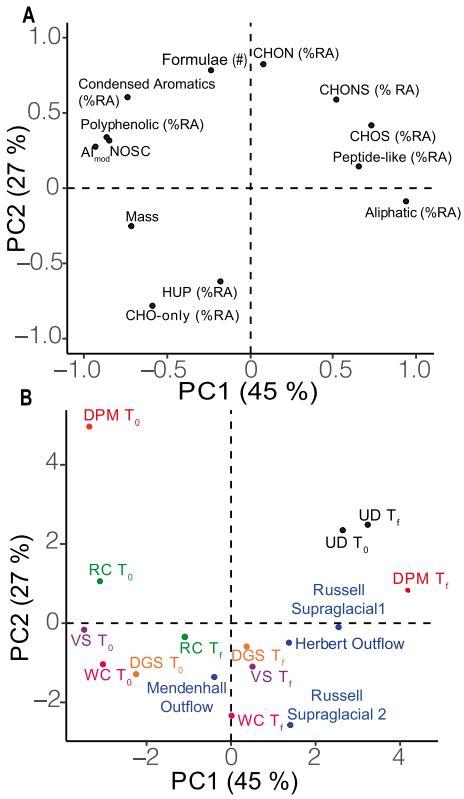

Figure 6. Principal component (PC) analysis detailing the relationship between glacial samples and endmember leachates pre- (T_0) and post-irradiation (T_f), based (a) Fourier transform ion cyclotron resonance mass spectrometry (FT-ICR MS) parameters. (b) Shows the relative positioning of all samples, highlighting the shift in molecular level composition of post-irradiation leachates toward glacial samples. Sample IDs are abbreviated in (b) and detailed within Section 2.1 of the Materials and Methods.

common photoproduced formulae (i.e., those only present after irradiation) had high H/C ratios (mean H/C 1.5 ± 0.13) and were found in aliphatic regions of van Krevelen space (Figure 5c). The vast majority (97%) of common photoresistant formulae (i.e., present pre- and post-irradiation) were HUP, where 37% and 76% of these formulae, respectively overlapped with the area in van Krevelen space attributed to the "island of stability" (Lechtenfeld et al., 2014) and carboxylic-rich alicyclic molecules (CRAM; Hertkorn et al., 2006, Figure 5d). For each endmember, some photoresistant molecular formulae, including CRAM formulae and those in the "island of stability," changed in RA upon irradiation, with increases typically focused on molecular formulae with high H/C ratios (Figure S1). Despite this, when all endmembers are compared together, there is no significant change in the RA of HUP compounds as a result of photodegradation (mean pre- and post-irradiation 54.6% and 63.1% RA, respectively, p-value 0.31; Table S2). The removal of polyphenolic and aromatic compounds, alongside the production of aliphatics, has been observed previously for DOM photodegradation studies in aquatic environments (Antony et al., 2018; Bostick et al., 2020; Gonsior et al., 2009; Stubbins et al., 2010), and supports the findings shared here. Overall, photodegradation caused a shift in molecular composition to higher H/C ratios for all endmembers, and produced relatively aliphatic enriched DOM (Figures 2–5 and S1).

3.4. Compositional Convergence Between Irradiated Endmembers and Glacial Samples

Concentrations of DOC remained higher in post-irradiation leachates than in glacial samples (Table S1, Figure 3a). The low DOC concentrations typically found in glacial ecosystems are due to limited OM available for leaching (i.e., no soils or litter layers) in comparison to other terrestrial environments, and due to dilution by large volumes of rain, snow, and meltwater (Boix Canadell et al., 2019; Hood et al., 2020). The lack of convergence of DOC concentrations between post-irradiated endmembers and glacial samples does not negatively impact our interpretation of the compositional shifts in DOM following irradiation, as the composition of DOM would remain the same if diluted with pure water (i.e., dilution with DOM-free water would lower the DOC concentration but DOM composition would not change).

It was hypothesized that after photodegradation endmember leachates would converge toward the aliphatic molecular level composition of glacial samples. Several univariate comparisons indicated that the molecular level composition of post-irradiation leachates converged with glacial samples (Table S2, Figures 3 and 4). In order to comprehensively assess the convergence, all FT-ICR MS variables were used in a multivariate PC analysis (see Section 2.6 for further description; Table S3, Figure 6a). Glacier samples generally occupied the bottom right quadrant (except for the Mendenhall Outflow) of the PC1 versus PC2 plot (Figure 6b). Initial endmember leachates were distributed in this PC space, and generally migrated toward the glacier samples post-irradiation. Exploring the PC analysis further, PC1 explained 45% of the variation in the data set and had a strong positive association with the RA of aliphatic and peptide-like compounds, and a strong negative association with mean mass, AI_{mod}, NOSC, and the RA of polyphenolics and condensed aromatics (Table S3, Figure 6a).

Photodegradation shifted all endmembers to more positive PC1 values (Figure 6b). This represented the decline in mass, AI_{mod}, NOSC, polyphenolics (% RA) and condensed aromatics (% RA), concurrent with the increase in the RA of aliphatic and peptide-like formulae in most endmembers (Table 1). It should be noted that the NOSC declined post-irradiation in most endmembers, but remained higher than glacial samples for all the endmember leachates (Table 1, Figure 3d). Additionally, when all leachates were compared together, peptide-like contributions were not significantly different between glacier samples and either pre- or post-irradiation leachates (p-value 0.17 and 0.29, respectively; Table S2, Figure 4d). This is due to the high RA of peptide-like formulae

in UD pre-irradiation (4.0% RA, mean of pre-irradiation leachates 0.7 ± 1.6% RA), in combination with the large variability in RA of peptide-like formulae found between glacial samples (mean 3.1 ± 2.5% RA; Table 1). PC2 explained less variation (27%) and was positively associated with the RA of CHON compounds and was negatively associated with the RA of CHO-only and HUP compounds (Table S3, Figure 6a). Most endmember leachates shifted toward more negative values on PC2 as a result of photodegradation (Figure 6b), reflecting the production of molecular formulae with a lower NOSC and increase in HUP compounds (% RA) in certain endmembers (Table 1).

Although trends in DOM compositional shifts were consistent for all leachates, unlike the other leachates UD was situated at positive values on PC1 pre-irradiation and exhibited the smallest shift along PC1 upon photodegradation (Figure 6b). Before irradiation UD had a high RA of aliphatic (31.9% RA, compared to the mean of 2.0% RA for other leachates) and peptide-like compounds, as well as a low RA of condensed aromatics (1.9% RA, compared to the mean of 13% RA for other leachates; Table 1) compared to other endmembers. Pre-irradiation UD was the most comparable endmember to the glacial samples and hence it was initially situated at positive values of PC1 (Figure 6b). The initial composition of UD likely reflects a mixture of different OM sources, including those that have already been exposed to ultraviolet light during atmospheric transport (Currie et al., 2002; Li et al., 2020). The lack of aromatic OM initially present in UD is likely to explain the minimal impact of photodegradation on its aliphatic content; hence, the lack of movement in PC space, in comparison to the other endmember sources. Furthermore, PC analysis is constrained to the major variability within the data set, in this case the increased RA of aliphatics post-photodegradation (Table S3). Consequently, despite photodegradation impacting the molecular composition of UD (e.g., increasing the RA of aliphatic, peptide-like, and sugar-like compounds and decreasing the RA of condensed aromatics and polyphenolics; Table 1), these compositional changes are muted in comparison to changes in the other endmembers. In general, photodegradation caused the molecular level composition of leachates to become more similar to glacier runoff (particularly with regard to the % RA of aliphatic, aromatic and polyphenolic compounds).

The compositional convergence of endmember sources post-irradiation with glacial DOM is apparent in van Krevelen space (Figures 2 and 5, and S1). By comparing common photoproduced and resistant molecular formulae (Figures 5c and 5d) with the core glacier signature (Figure 5a) it is apparent that photodegradation of all endmembers produced DOM resembling that found in glacial runoff. Bray Curtis analysis revealed two distinct clusters of samples, with post-irradiation leachates having more common molecular formulae with the core glacier signature and glacier samples than pre-irradiation leachates (Figures 7 and S2). Unsurprisingly, due to its aliphatic-enriched molecular signature pre-irradiation UD was situated close to post-irradiation leachates and the core glacier signature. Post-irradiation RC was situated in the cluster associated with pre-irradiation leachates (Figure 7). This is because after photodegradation, RC still had a substantial RA of aromatic and polyphenolic formulae (combined 22.2% RA), compared to other post-irradiation leachates (mean 5.9 ± 7.1% RA; Table 1). RC had several photoproduced and resistant molecular formulae which were aromatic (Figure S1), these compounds could be newly formed (e.g., via reactions between lignin and reactive oxygen species, like hydroxyl radicals generated during photochemical degradation) or detected post-irradiation due to changes in ionization efficiency (Chen et al., 2014; Waggoner et al., 2015, 2017). When examined against individual glacier samples (Figure S2), post-irradiation RC appears similar to Herbert and Mendenhall Glacier. These glacier catchments have enhanced aromatic inputs, compared to other glacier sites as evidenced by direct allochthonous inputs from forested slopes and nunataks above the glaciers (Behnke et al., 2020; Spencer, Vermilyea, et al., 2014). Although past studies have highlighted photoproduced aromatics may represent a source of this material, particularly in the presence of iron (Chen et al., 2014; Cwiertny et al., 2008); in all cases, the net change in molecular composition following photodegradation is toward aliphatic enrichment (Chen et al., 2014; Waggoner et al., 2015, 2017). This corroborates that a substantial portion of the molecular composition observed in glacier ecosystems could be formed through photodegradation of allochthonous OM sources, explaining the close similarity in molecular formulae between photodegraded leachates and the glacier runoff samples examined here.

To further assess this similarity between post-irradiation leachates and the core glacier signature further, we compared the percent overlap of molecular formulae present between the core glacier signature and each post-irradiation leachate. There was substantial overlap in the molecular formulae present after photodegradation with the core glacier signature (median of 84%, range of 76%–95%; Figures 7 and S3). Importantly, photodegradation produced 36% of the aliphatic molecular formulae present in the core glacier signature (range 4.5%–79%),

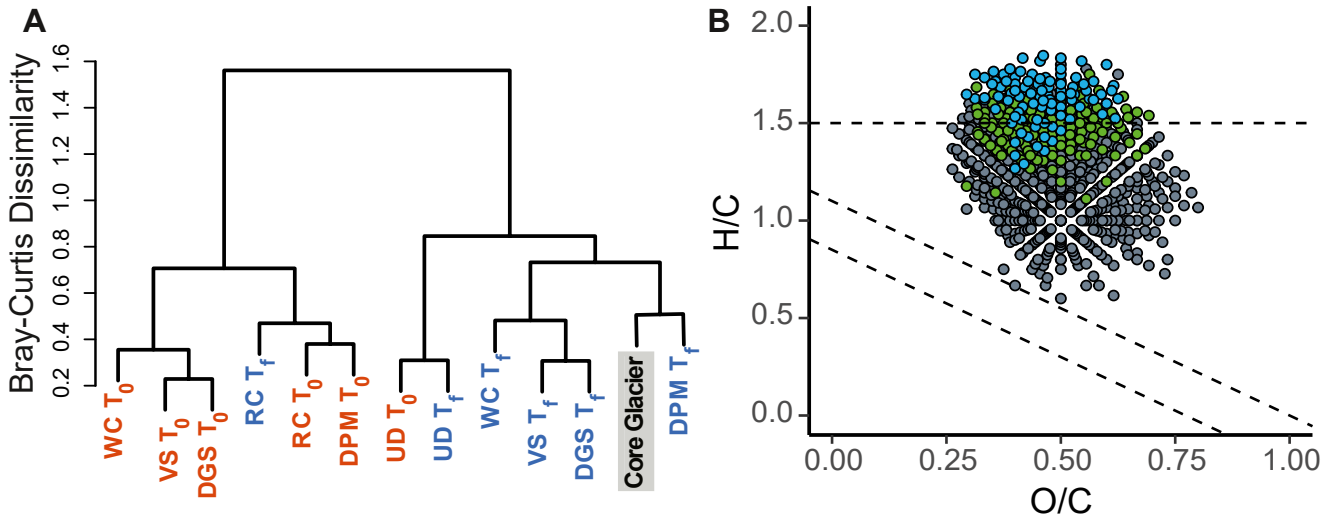

Figure 7. (a) Dendrogram showing results of Bray-Curtis dissimilarity index, sample clustering based on the ward method. Dissimilarity was calculated based on the presence and absence of individual formulae identified by Fourier transform ion cyclotron resonance mass spectrometry (FT-ICR MS; samples with more common formulae are listed on branches closer together). (b) Combined van Krevelen diagram for all endmember leachates, showing common molecular formulae that are present across four or more endmember leachates, which are categorized as either photoresistant or produced, and are present in the core glacier signature. Colors represent the dominant photodegradation category. Gray: in most endmember leachates, the molecular formula is categorized as photoresistant. Blue: the majority categorize formula as photoproduced. Green: same number of samples have molecular formula categorized as photoproduced as resistant.

totaling a median overlap of 74% (range 47%–89%) of the aliphatic formulae in the core glacier signature with photodegraded endmembers (Figure S3). Both similarity metrics (i.e., Bray Curtis and % overlap) yielded different results, suggesting different endmembers are most alike the core glacier signature (Figures 7, S2, and S3). This disparity was unsurprising given that Bray Curtis considers all molecular formulae across endmembers and the glacial samples, whereas the percentage overlap confines the comparison to only those formulae present in the core glacier signature. Considering this, together with the assessments having been based only on presence/absence of different molecular formulae rather than RA, and that glacier DOM is likely a mixture of different allochthonous and autochthonous OM sources which may vary, and in proportions thereof, between different regions and glacier ecosystems (i.e., our six endmember sources may not encompass the full range of OM available to glacier surfaces; Fellman, Hood, Raymond, Stubbins, & Spencer, 2015; Lawson, Bhatia, et al., 2014; Singer et al., 2012; Smith et al., 2018), it is inappropriate to stipulate which of the endmembers examined here is solely most like DOM in glacier runoff. Nonetheless, the dramatic shifts in molecular composition and remarkable similarity in molecular formulae between post-irradiation leachates, and supraglacial and bulk runoff samples highlights that photodegradation may be responsible for the production of a substantial portion of the compositionally distinct DOM seen in glacier runoff.

3.5. The Role of Photochemistry in the Formation of Glacial DOM Molecular Properties

Our findings suggest that photochemical reactions may represent a pathway for the transformation of allochthonous, aromatic-rich OM sources toward the aliphatic and protein-rich composition observed for glacier DOM (Antony et al., 2014; Bhatia et al., 2010; Lawson, Bhatia, et al., 2014; Singer et al., 2012; Spencer, Guo, et al., 2014; Stubbins, Hood, et al., 2012). However, further research is required to assess the importance of this mechanism under more environmentally relevant conditions and in relation to other glacier biogeochemical processes. Although our experiments were conducted in the aqueous phase, photodegradation of OM within solid ice or snow, and in the atmosphere (i.e., bound to aerosols, in aqueous phase or on ice crystal surfaces) has also been shown to be extensive, and despite the chemical degradation pathways being diverse (especially during atmospheric transport, e.g., due to direct photolysis and indirect photooxidation), photochemical reactions across these environments have been shown to breakdown aromatic organic molecules (Antony et al., 2018; Domine et al., 2013; George et al., 2015; Kahan & Donaldson, 2007; Romonosky et al., 2015) as observed in this study. Differences in chemical pathways between these environments and phases may result in variances in the DOM chemistry and thus the observed photoproduced and photoresistant compounds, compared to those seen here

under aqueous conditions. Assessing the major site of transformation, differences in photochemical reactions between phases and rates of reaction possible in transit to, and on, the glacier surface was beyond the scope of this study. That said, our data suggest that a large proportion of observed glacier DOM molecular signatures could result from photodegradation of allochthonous, aromatic-rich OM. Additionally, the similarity between the composition of DOM of pre-irradiation UD, and more broadly DOM in precipitation and WSOM from aerosols, with that in our supra- and subglacial runoff samples suggests that much of the transformation of allochthonous OM may occur during atmospheric transport (Fellman, Hood, Raymond, Stubbins, & Spencer, 2015; Gurganus et al., 2015; Li et al., 2018; Spencer, Guo, et al., 2014; Spencer, Vermilyea, et al., 2014; Wozniak et al., 2008).

To date, microbial production and metabolism of OM has been suggested as the primary reason for the aliphatic-rich DOM composition in glacial runoff (Bhatia et al., 2010; Lawson, Bhatia, et al., 2014). This is because microbial activity has been shown to be extensive in some glacier ecosystems, and microbial productivity has been positively correlated with the concentration of biolabile DOM species in supraglacial runoff (Musilova et al., 2017; Smith et al., 2017; Wadham et al., 2004; Zhou, Zhou, Hu, et al., 2019). Here, we demonstrate that photochemical alteration of allochthonous OM could account for the distinct molecular signature of glacier DOM. Given that some of these allochthonous inputs include aged OM sources, such as fossil fuel combustion byproducts, the photodegradation pathway could also account for the aged signature reported for glacier DOC (Aiken et al., 2014; Andrews et al., 2018; Bhatia et al., 2013; Fellman, Hood, Raymond, Stubbins, & Spencer, 2015; Hood et al., 2009; Spencer, Guo, et al., 2014). Dependent on glacier DOC age (749–10,824 years), and assuming derivation from only modern OM or a ^{14}C dead fossil fuel source, across glacier ecosystems and regions it is estimated that 9%–73% of glacier DOC could originate from fossil fuels combustion byproducts, producing its distinct molecular fingerprint (Fellman, Hood, Raymond, Stubbins, & Spencer, 2015; Spencer, Guo, et al., 2014; Stubbins, Hood, et al., 2012). Therefore, we do not suggest that microbial autochthonous production and metabolism does not contribute aliphatic and protein-like DOM to the glacier DOM pool, since glacier DOM is likely a mixture of different OM sources. Rather, our results suggest that photodegradation may have the ability to produce a proportion of glacier DOM derived from aromatic allochthonous sources.

Glacier-derived DOM is highly bioavailable and ancient (Hood et al., 2009; Singer et al., 2012; Spencer, Guo, et al., 2014; Zhou, Zhou, Hu, et al., 2019). It remains to be determined whether the sources of OM studied here are bioavailable post-irradiation. Nevertheless, many of the molecular formulae present after photodegradation have H/C ratios greater than the "molecular lability boundary" (≥1.5 H/C; Table 1, Figure 5c, D'Andrilli et al., 2015). Thus, it appears likely that photodegradation may increase the biolability of the endmembers used in this study. Photodegradation of aromatic DOM has been shown to stimulate bacterial production in other aquatic environments (Lindell et al., 1995; Moran & Zepp, 1997). Similarly, snow pack analysis has shown that photodegradation enhances the bioavailability of organic nitrogen and phosphorus (Antony et al., 2018). Potentially biolabile, aliphatic molecular formulae are observed across all the endmember sources we studied, regardless of the age of the carbon source (Figures 5c and S1). Many of these molecular formulae (up to 89%) are present in the core glacier signature (Figures 7 and S3). Thus, photodegradation of aged sources, such as DPM (^{14}C dead), together with fractions of proglacial soil and UD, could explain the ancient, yet highly bioavailable, component of DOM observed across glacial ecosystems. Anthropogenic aerosols have been cited as the source of ancient, biolabile carbon to glacier surfaces and outflows (Fellman, Hood, Raymond, Stubbins, & Spencer, 2015; Spencer, Guo, et al., 2014; Stubbins, Hood, et al., 2012). In this study, we highlight a mechanism that may account for the concurrent aliphatic and protein-rich DOM composition.

Results from this study suggest that photochemical transformations of allochthonous OM may mediate the composition of DOM found in glacier ecosystems. Further research is required to understand the relative importance of this mechanism in relation to other biogeochemical processes at play on the ice surface and at the glacier bed; this includes quantifying the rates and magnitudes of photodegradation possible in transit to, and on, glacier surfaces. However, given the intense ultraviolet conditions of atmospheric transit and on ice surfaces, photochemical alteration of DOM has the potential to be significant. These results underscore the complexity in deciphering the origin of OM to glacier ecosystems: the remote nature, long atmospheric transport distance, together with the high intensities of ultraviolet light (both in atmospheric transport and in supraglacial environments), could lead to seemingly homogenous, aliphatic-enriched molecular signatures regardless of DOM source. As such, we encourage photodegradation processes be considered when assessing glacier DOM source.

Data Availability Statement

Data related to this publication are available through www.earthchem.org using the following DOI: https://doi.org/10.26022/IEDA/111996. Raw FT-ICR MS files can be accessed through DOI: https://doi.org/10.17605/OSF.IO/D57K9

Acknowledgments
Megan I. Behnke is thanked for collecting the Alaskan soil samples, Stephanie McColaugh for collecting the Russell Glacier samples, Casey Luzius for help with leachate preparations, and Sarah Ellen Johnston for assistance with DOC analyses. Funding Source: This study was supported by NSF, DEB 1145932 and OCE 1333157 to R. G. M. Spencer. Funding was provided by Alaska EPSCoR (OIA-1757348). A portion of this work was performed in the Ion Cyclotron Resonance User Facility at the National High Magnetic Field Laboratory, which is supported by the National Science Foundation Division of Chemistry and Division of Materials Research through DMR 16-44779, and the State of Florida.

References

Aiken, G. R., Spencer, R. G., Striegl, R. G., Schuster, P. F., & Raymond, P. A. (2014). Influences of glacier melt and permafrost thaw on the age of dissolved organic carbon in the Yukon River basin. *Global Biogeochemical Cycles*, *28*(5), 525–537. https://doi.org/10.1002/2013gb004764

Andrews, M. G., Jacobson, A. D., Osburn, M. R., & Flynn, T. M. (2018). Dissolved carbon dynamics in meltwaters from the Russell Glacier, Greenland Ice Sheet. *Journal of Geophysical Research: Biogeosciences*, *123*(9), 2922–2940. https://doi.org/10.1029/2018jg004458

Antony, R., Grannas, A. M., Willoughby, A. S., Sleighter, R. L., Thamban, M., & Hatcher, P. G. (2014). Origin and sources of dissolved organic matter in snow on the East Antarctic ice sheet. *Environmental Science & Technology*, *48*(11), 6151–6159. https://doi.org/10.1021/es405246a

Antony, R., Willoughby, A. S., Grannas, A. M., Catanzano, V., Sleighter, R. L., Thamban, M., et al. (2017). Molecular insights on dissolved organic matter transformation by supraglacial microbial communities. *Environmental Science & Technology*, *51*(8), 4328–4337. https://doi.org/10.1021/acs.est.6b05780

Antony, R., Willoughby, A. S., Grannas, A. M., Catanzano, V., Sleighter, R. L., Thamban, M., & Hatcher, P. G. (2018). Photo-biochemical transformation of dissolved organic matter on the surface of the coastal East Antarctic ice sheet. *Biogeochemistry*, *141*(2), 229–247. https://doi.org/10.1007/s10533-018-0516-0

Bardgett, R. D., Richter, A., Bol, R., Garnett, M. H., Bäumler, R., Xu, X., et al. (2007). Heterotrophic microbial communities use ancient carbon following glacial retreat. *Biology Letters*, *3*(5), 487–490. https://doi.org/10.1098/rsbl.2007.0242

Barker, J. D., Sharp, M., & Turner, R. (2009). Using synchronous fluorescence spectroscopy and principal components analysis to monitor dissolved organic matter dynamics in a glacier system. *Hydrological Processes: International Journal*, *23*(10), 1487–1500. https://doi.org/10.1002/hyp.7274

Behnke, M., McClelland, J., Tank, S., Kellerman, A., Holmes, R., Haghipour, N., et al. (2021). Pan-Arctic riverine dissolved organic matter: Synchronous molecular stability, shifting sources and subsidies. *Global Biogeochemical Cycles*, *35*(4), e2020GB006871. https://doi.org/10.1029/2020gb006871

Behnke, M. I., Stubbins, A., Fellman, J. B., Hood, E., Dittmar, T., & Spencer, R. G. (2020). Dissolved organic matter sources in glacierized watersheds delineated through compositional and carbon isotopic modeling. *Limnology & Oceanography*, *66*. https://doi.org/10.1002/lno.11615

Bertilsson, S., & Tranvik, L. J. (2000). Photochemical transformation of dissolved organic matter in lakes. *Limnology & Oceanography*, *45*(4), 753–762. https://doi.org/10.4319/lo.2000.45.4.0753

Bhatia, M. P., Das, S. B., Longnecker, K., Charette, M. A., & Kujawinski, E. B. (2010). Molecular characterization of dissolved organic matter associated with the Greenland ice sheet. *Geochimica et Cosmochimica Acta*, *74*(13), 3768–3784. https://doi.org/10.1016/j.gca.2010.03.035

Bhatia, M. P., Das, S. B., Xu, L., Charette, M. A., Wadham, J. L., & Kujawinski, E. B. (2013). Organic carbon export from the Greenland ice sheet. *Geochimica et Cosmochimica Acta*, *109*, 329–344. https://doi.org/10.1016/j.gca.2013.02.006

Bird, M. I., Wynn, J. G., Saiz, G., Wurster, C. M., & McBeath, A. (2015). The pyrogenic carbon cycle. *Annual Review of Earth and Planetary Sciences*, *43*, 273–298. https://doi.org/10.1146/annurev-earth-060614-105038

Boix Canadell, M., Escoffier, N., Ulseth, A. J., Lane, S. N., & Battin, T. J. (2019). Alpine glacier shrinkage drives shift in dissolved organic carbon export from quasi-chemostasis to transport limitation. *Geophysical Research Letters*, *46*(15), 8872–8881. https://doi.org/10.1029/2019gl083424

Bostick, K. W., Zimmerman, A. R., Goranov, A. I., Mitra, S., Hatcher, P. G., & Wozniak, A. S. (2020). Photolability of pyrogenic dissolved organic matter from a thermal series of laboratory-prepared chars. *The Science of the Total Environment*, *724*, 138198. https://doi.org/10.1016/j.scitotenv.2020.138198

Chen, H., Abdulla, H. A., Sanders, R. L., Myneni, S. C., Mopper, K., & Hatcher, P. G. (2014). Production of black carbon-like and aliphatic molecules from terrestrial dissolved organic matter in the presence of sunlight and iron. *Environmental Science and Technology Letters*, *1*(10), 399–404. https://doi.org/10.1021/ez5002598

Chen, M., & Jaffé, R. (2014). Photo-and bio-reactivity patterns of dissolved organic matter from biomass and soil leachates and surface waters in a subtropical wetland. *Water Research*, *61*, 181–190. https://doi.org/10.1016/j.watres.2014.03.075

CIE. (1989). *No. 85 technical report: Solar spectral irradiance* (1st edn).

Currie, L. A., Benner, B. A., Jr, Kessler, J., Klinedinst, D., Klouda, G., Marolf, J., et al. (2002). A critical evaluation of interlaboratory data on total, elemental, and isotopic carbon in the carbonaceous particle reference material, NIST SRM 1649a. *Journal of Research of the National Institute of Standards and Technology*, *107*(3), 279. https://doi.org/10.6028/jres.107.022

Cwiertny, D. M., Young, M. A., & Grassian, V. H. (2008). Chemistry and photochemistry of mineral dust aerosol. *Annual Review of Physical Chemistry*, *59*, 27–51. https://doi.org/10.1146/annurev.physchem.59.032607.093630

D'Andrilli, J., Cooper, W. T., Foreman, C. M., & Marshall, A. G. (2015). An ultrahigh-resolution mass spectrometry index to estimate natural organic matter lability. *Rapid Communications in Mass Spectrometry*, *29*(24), 2385–2401. https://doi.org/10.1002/rcm.7400

Dittmar, T., Koch, B., Hertkorn, N., & Kattner, G. (2008). A simple and efficient method for the solid-phase extraction of dissolved organic matter (SPE-DOM) from seawater. *Limnology and Oceanography: Methods*, *6*(6), 230–235. https://doi.org/10.4319/lom.2008.6.230

Domine, F., Bock, J., Voisin, D., & Donaldson, D. (2013). Can we model snow photochemistry? Problems with the current approaches. *The Journal of Physical Chemistry A*, *117*(23), 4733–4749. https://doi.org/10.1021/jp3123314

Fellman, J. B., Hood, E., Raymond, P. A., Hudson, J., Bozeman, M., & Arimitsu, M. (2015). Evidence for the assimilation of ancient glacier organic carbon in a proglacial stream food web. *Limnology & Oceanography*, *60*(4), 1118–1128. https://doi.org/10.1002/lno.10088

Fellman, J. B., Hood, E., Raymond, P. A., Stubbins, A., & Spencer, R. G. (2015). Spatial variation in the origin of dissolved organic carbon in snow on the Juneau icefield, Southeast Alaska. *Environmental Science & Technology*, *49*(19), 11492–11499. https://doi.org/10.1021/acs.est.5b02685

Fellman, J. B., Hood, E., Spencer, R. G., Stubbins, A., & Raymond, P. A. (2014). Watershed glacier coverage influences dissolved organic matter biogeochemistry in coastal watersheds of southeast Alaska. *Ecosystems*, *17*(6), 1014–1025. https://doi.org/10.1007/s10021-014-9777-1

Fellman, J. B., Petrone, K. C., & Grierson, P. F. (2013). Leaf litter age, chemical quality, and photodegradation control the fate of leachate dissolved organic matter in a dryland river. *Journal of Arid Environments*, *89*, 30–37. https://doi.org/10.1016/j.jaridenv.2012.10.011

Ferrario, C., Pittino, F., Tagliaferri, I., Gandolfi, I., Bestetti, G., Azzoni, R. S., et al. (2017). Bacteria contribute to pesticide degradation in cryoconite holes in an Alpine glacier. *Environmental Pollution*, *230*, 919–926. https://doi.org/10.1016/j.envpol.2017.07.039

Franzetti, A., Tagliaferri, I., Gandolfi, I., Bestetti, G., Minora, U., Mayer, C., et al. (2016). Light-dependent microbial metabolisms drive carbon fluxes on glacier surfaces. *The ISME Journal*, *10*(12), 2984–2988. https://doi.org/10.1038/ismej.2016.72

George, C., Ammann, M., D'Anna, B., Donaldson, D., & Nizkorodov, S. A. (2015). Heterogeneous photochemistry in the atmosphere. *Chemical Reviews*, *115*(10), 4218–4258. https://doi.org/10.1021/cr500648z

Gomez-Saez, G. V., Pohlabeln, A. M., Stubbins, A., Marsay, C. M., & Dittmar, T. (2017). Photochemical alteration of dissolved organic sulfur from sulfidic porewater. *Environmental Science & Technology*, *51*(24), 14144–14154. https://doi.org/10.1021/acs.est.7b03713

Gonsior, M., Peake, B. M., Cooper, W. T., Podgorski, D., D'Andrilli, J., & Cooper, W. J. (2009). Photochemically induced changes in dissolved organic matter identified by ultrahigh resolution Fourier transform ion cyclotron resonance mass spectrometry. *Environmental Science & Technology*, *43*(3), 698–703. https://doi.org/10.1021/es8022804

Goslee, S. C., & Urban, D. L. (2007). The ecodist package for dissimilarity-based analysis of ecological data. *Journal of Statistical Software*, *22*(7), 1–19. https://doi.org/10.18637/jss.v022.i07

Grannas, A., Jones, A. E., Dibb, J., Ammann, M., Anastasio, C., Beine, H., et al. (2007). An overview of snow photochemistry: Evidence, mechanisms and impacts. *Atmospheric Chemistry and Physics*, *7*(16), 4329–4373. https://doi.org/10.5194/acp-7-4329-2007

Grannas, A. M., Bogdal, C., Hageman, K. J., Halsall, C., Harner, T., Hung, H., et al. (2013). The role of the global cryosphere in the fate of organic contaminants. *Atmospheric Chemistry and Physics*, *13*(6), 3271–3305. https://doi.org/10.5194/acp-13-3271-2013

Grannas, A. M., Shepson, P. B., & Filley, T. R. (2004). Photochemistry and nature of organic matter in Arctic and Antarctic snow. *Global Biogeochemical Cycles*, *18*(1). https://doi.org/10.1029/2003gb002133

Gurganus, S. C., Wozniak, A. S., & Hatcher, P. G. (2015). Molecular characteristics of the water soluble organic matter in size-fractionated aerosols collected over the North Atlantic Ocean. *Marine Chemistry*, *170*, 37–48. https://doi.org/10.1016/j.marchem.2015.01.007

Hammes, K., Smernik, R. J., Skjemstad, J. O., Herzog, A., Vogt, U. F., & Schmidt, M. W. (2006). Synthesis and characterisation of laboratory-charred grass straw (Oryza sativa) and chestnut wood (Castanea sativa) as reference materials for black carbon quantification. *Organic Geochemistry*, *37*(11), 1629–1633. https://doi.org/10.1016/j.orggeochem.2006.07.003

Hansen, A. M., Kraus, T. E., Pellerin, B. A., Fleck, J. A., Downing, B. D., & Bergamaschi, B. A. (2016). Optical properties of dissolved organic matter (DOM): Effects of biological and photolytic degradation. *Limnology & Oceanography*, *61*(3), 1015–1032. https://doi.org/10.1002/lno.10270

Helms, J. R., Stubbins, A., Ritchie, J. D., Minor, E. C., Kieber, D. J., & Mopper, K. (2008). Absorption spectral slopes and slope ratios as indicators of molecular weight, source, and photobleaching of chromophoric dissolved organic matter. *Limnology & Oceanography*, *53*(3), 955–969. https://doi.org/10.4319/lo.2008.53.3.0955

Hemingway, J. D., Spencer, R. G., Podgorski, D. C., Zito, P., Sen, I. S., & Galy, V. V. (2019). Glacier meltwater and monsoon precipitation drive Upper Ganges Basin dissolved organic matter composition. *Geochimica et Cosmochimica Acta*, *244*, 216–228. https://doi.org/10.1016/j.gca.2018.10.012

Herbert, B., Villa, S., & Halsall, C. (2006). Chemical interactions with snow: Understanding the behavior and fate of semi-volatile organic compounds in snow. *Ecotoxicology and Environmental Safety*, *63*(1), 3–16. https://doi.org/10.1016/j.ecoenv.2005.05.012

Hertkorn, N., Benner, R., Frommberger, M., Schmitt-Kopplin, P., Witt, M., Kaiser, K., et al. (2006). Characterization of a major refractory component of marine dissolved organic matter. *Geochimica et Cosmochimica Acta*, *70*(12), 2990–3010. https://doi.org/10.1016/j.gca.2006.03.021

Holland, A. T., Williamson, C. J., Sgouridis, F., Tedstone, A. J., McCutcheon, J., Cook, J. M., et al. (2019). Dissolved organic nutrients dominate melting surface ice of the Dark Zone (Greenland Ice Sheet). *Biogeosciences*, *16*(16), 3283–3296. https://doi.org/10.5194/bg-16-3283-2019

Hood, E., Battin, T., Fellman, J., O'Neel, S., & Spencer, R. (2015). Storage and release of organic carbon from glaciers and ice sheets. *Nature Geoscience*, *8*, 91–96. https://doi.org/10.1038/ngeo2331

Hood, E., Fellman, J., Spencer, R., Hernes, P., Edwards, R., D'Amore, D., & Scott, D. (2009). Glaciers as a source of ancient and labile organic matter to the marine environment. *Letters to Nature*, *462*(24), 1044–1048. https://doi.org/10.1038/nature08580

Hood, E., Fellman, J. B., & Spencer, R. G. (2020). Glacier loss impacts riverine organic carbon transport to the ocean. *Geophysical Research Letters*, *47*(19), e2020GL089804. https://doi.org/10.1029/2020gl089804

Hu, C., Muller-Karger, F. E., & Zepp, R. G. (2002). Absorbance, absorption coefficient, and apparent quantum yield: A comment on common ambiguity in the use of these optical concepts. *Limnology & Oceanography*, *47*(4), 1261–1267. https://doi.org/10.4319/lo.2002.47.4.1261

Kahan, T., & Donaldson, D. (2007). Photolysis of polycyclic aromatic hydrocarbons on water and ice surfaces. *The Journal of Physical Chemistry A*, *111*(7), 1277–1285. https://doi.org/10.1021/jp066660t

Kellerman, A., Hawkings, J., Wadham, J., Kohler, T., Stibal, M., Grater, E., et al. (2020). Glacier outflow dissolved organic matter as a window into seasonally changing carbon sources: Leverett Glacier, Greenland. *Journal of Geophysical Research: Biogeosciences*, *125*, e2019JG005161. https://doi.org/10.1029/2019jg005161

Kellerman, A. M., Vonk, J., McColaugh, S., Podgorski, D. C., van Winden, E., Hawkings, J. R., et al. (2021). Molecular signatures of glacial dissolved organic matter from Svalbard and Greenland. *Global Biogeochemical Cycles*, *35*(3), e2020GB006709. https://doi.org/10.1029/2020gb006709

Kirillova, E. N., Andersson, A., Sheesley, R. J., Kruså, M., Praveen, P., Budhavant, K., et al. (2013). ^{13}C-and ^{14}C-based study of sources and atmospheric processing of water-soluble organic carbon (WSOC) in South Asian aerosols. *Journal of Geophysical Research*, *118*(2), 614–626. https://doi.org/10.1002/jgrd.50130

Klán, P., Klánová, J., Holoubek, I., & Čupr, P. (2003). Photochemical activity of organic compounds in ice induced by sunlight irradiation: The Svalbard project. *Geophysical Research Letters*, *30*(6).

Koch, B., & Dittmar, T. (2006). From mass to structure: An aromaticity index for high-resolution mass data of natural organic matter. *Rapid Communications in Mass Spectrometry*, *20*(5), 926–932. https://doi.org/10.1002/rcm.2386

Koch, B., & Dittmar, T. (2016). From mass to structure: An aromaticity index for high-resolution mass data of natural organic matter. *Rapid Communications in Mass Spectrometry*, *30*. https://doi.org/10.1002/rcm.7433

Kurek, M. R., Poulin, B. A., McKenna, A. M., & Spencer, R. G. (2020). Deciphering dissolved organic matter: Ionization, dopant, and fragmentation insights via Fourier transform-ion cyclotron resonance mass spectrometry. *Environmental Science & Technology*, *54*(24), 16249–16259. https://doi.org/10.1021/acs.est.0c05206

Laurion, I., & Mladenov, N. (2013). Dissolved organic matter photolysis in Canadian arctic thaw ponds. *Environmental Research Letters*, *8*(3), 035026. https://doi.org/10.1088/1748-9326/8/3/035026

Lawson, E. C., Bhatia, M. P., Wadham, J. L., & Kujawinski, E. B. (2014). Continuous summer export of nitrogen-rich organic matter from the Greenland Ice Sheet inferred by ultrahigh resolution mass spectrometry. *Environmental Science & Technology*, *48*(24), 14248–14257. https://doi.org/10.1021/es501732h

Lawson, E. C., Wadham, J. L., Tranter, M., Stibal, M., Lis, G. P., Butler, C. E., et al. (2014). Greenland Ice Sheet exports labile organic carbon to the Arctic oceans. *Biogeosciences*, *11*(14), 4015–4028. https://doi.org/10.5194/bg-11-4015-2014

Lê, S., Josse, J., & Husson, F. (2008). FactoMineR: An R package for multivariate analysis. *Journal of Statistical Software*, *25*(1).

Lechtenfeld, O. J., Kattner, G., Flerus, R., McCallister, S. L., Schmitt-Kopplin, P., & Koch, B. P. (2014). Molecular transformation and degradation of refractory dissolved organic matter in the Atlantic and Southern Ocean. *Geochimica et Cosmochimica Acta*, *126*, 321–337. https://doi.org/10.1016/j.gca.2013.11.009

Li, C., Chen, P., Kang, S., Yan, F., Tripathee, L., Wu, G., et al. (2018). Fossil fuel combustion emission from South Asia influences precipitation dissolved organic carbon reaching the remote Tibetan plateau: Isotopic and molecular evidence. *Journal of Geophysical Research: Atmospheres*, *123*(11), 6248–6258. https://doi.org/10.1029/2017jd028181

Li, S., Fan, R., Luo, D., Xue, Q., Li, L., Yu, X., et al. (2020). Variation in quantity and quality of rainwater dissolved organic matter (DOM) in a peri-urban region: Implications for the effect of seasonal patterns on DOM fates. *Atmospheric Environment*, *239*, 117769. https://doi.org/10.1016/j.atmosenv.2020.117769

Lindell, M. J., Granéli, W., & Tranvik, L. J. (1995). Enhanced bacterial growth in response to photochemical transformation of dissolved organic matter. *Limnology & Oceanography*, *40*(1), 195–199. https://doi.org/10.4319/lo.1995.40.1.0195

Mann, P., Davydova, A., Zimov, N., Spencer, R., Davydov, S., Bulygina, E., et al. (2012). Controls on the composition and lability of dissolved organic matter in Siberia's Kolyma River basin. *Journal of Geophysical Research: Biogeosciences*, *117*(G1). https://doi.org/10.1029/2011jg001798

Masiello, C. A. (2004). New directions in black carbon organic geochemistry. *Marine Chemistry*, *92*(1–4), 201–213. https://doi.org/10.1016/j.marchem.2004.06.043

Mazzoleni, L. R., Saranjampour, P., Dalbec, M. M., Samburova, V., Hallar, A. G., Zielinska, B., et al. (2012). Identification of water-soluble organic carbon in non-urban aerosols using ultrahigh-resolution FT-ICR mass spectrometry: Organic anions. *Environmental Chemistry*, *9*(3), 285–297. https://doi.org/10.1071/en11167

Milner, A. M., Fastie, C. L., Chapin, F. S., Engstrom, D. R., & Sharman, L. C. (2007). Interactions and linkages among ecosystems during landscape evolution. *BioScience*, *57*(3), 237–247. https://doi.org/10.1641/b570307

Moran, M. A., & Zepp, R. G. (1997). Role of photoreactions in the formation of biologically labile compounds from dissolved organic matter. *Limnology & Oceanography*, *42*(6), 1307–1316. https://doi.org/10.4319/lo.1997.42.6.1307

Musilova, M., Tranter, M., Wadham, J., Telling, J., Tedstone, A., & Anesio, A. M. (2017). Microbially driven export of labile organic carbon from the Greenland ice sheet. *Nature Geoscience*, *10*(5), 360. https://doi.org/10.1038/ngeo2920

Price, P., Rohde, R., & Bay, R. (2009). Fluxes of microbes, organic aerosols, dust, sea-salt Na ions, non-sea-salt Ca ions, and methanesulfonate onto Greenland and Antarctic ice. *Biogeosciences*, *6*(3), 479–486. https://doi.org/10.5194/bg-6-479-2009

R Core Team. (2020). *R: A language and environment for statistical computing*. R Foundation for Statistical Computing, Vienna.

Ram, K., & Anastasio, C. (2009). Photochemistry of phenanthrene, pyrene, and fluoranthene in ice and snow. *Atmospheric Environment*, *43*(14), 2252–2259. https://doi.org/10.1016/j.atmosenv.2009.01.044

Riedel, T., Biester, H., & Dittmar, T. (2012). Molecular fractionation of dissolved organic matter with metal salts. *Environmental Science & Technology*, *46*(8), 4419–4426. https://doi.org/10.1021/es203901u

Romonosky, D. E., Laskin, A., Laskin, J., & Nizkorodov, S. A. (2015). High-resolution mass spectrometry and molecular characterization of aqueous photochemistry products of common types of secondary organic aerosols. *The Journal of Physical Chemistry A*, *119*(11), 2594–2606. https://doi.org/10.1021/jp509476r

Savory, J. J., Kaiser, N. K., McKenna, A. M., Xian, F., Blakney, G. T., Rodgers, R. P., et al. (2011). Parts-per-billion Fourier transform ion cyclotron resonance mass measurement accuracy with a "walking" calibration equation. *Analytical Chemistry*, *83*(5), 1732–1736. https://doi.org/10.1021/ac102943z

Seidel, M., Yager, P. L., Ward, N. D., Carpenter, E. J., Gomes, H. R., Krusche, A. V., et al. (2015). Molecular-level changes of dissolved organic matter along the Amazon River-to-ocean continuum. *Marine Chemistry*, *177*, 218–231. https://doi.org/10.1016/j.marchem.2015.06.019

Singer, G. A., Fasching, C., Wilhelm, L., Niggemann, J., Steier, P., Dittmar, T., & Battin, T. J. (2012). Biogeochemically diverse organic matter in Alpine glaciers and its downstream fate. *Nature Geoscience*, *5*(10), 710. https://doi.org/10.1038/ngeo1581

Sleighter, R. L., & Hatcher, P. G. (2008). Molecular characterization of dissolved organic matter (DOM) along a river to ocean transect of the lower Chesapeake Bay by ultrahigh resolution electrospray ionization Fourier transform ion cyclotron resonance mass spectrometry. *Marine Chemistry*, *110*(3–4), 140–152. https://doi.org/10.1016/j.marchem.2008.04.008

Smith, H. J., Dieser, M., McKnight, D. M., SanClements, M., & Foreman, C. M. (2018). Relationship between dissolved organic matter quality and microbial community composition across polar glacial environments. *FEMS Microbiology Ecology*, *94*(7), fiy090. https://doi.org/10.1093/femsec/fiy090

Smith, H. J., Foster, R. A., McKnight, D. M., Lisle, J. T., Littmann, S., Kuypers, M. M., & Foreman, C. M. (2017). Microbial formation of labile organic carbon in Antarctic glacial environments. *Nature Geoscience*, *10*(5), 356–359. https://doi.org/10.1038/ngeo2925

Spencer, R. G., Guo, W., Raymond, P. A., Dittmar, T., Hood, E., Fellman, J., & Stubbins, A. (2014). Source and biolability of ancient dissolved organic matter in glacier and lake ecosystems on the Tibetan Plateau. *Geochimica et Cosmochimica Acta*, *142*, 64–74. https://doi.org/10.1016/j.gca.2014.08.006

Spencer, R. G., Mann, P. J., Dittmar, T., Eglinton, T. I., McIntyre, C., Holmes, R. M., et al. (2015). Detecting the signature of permafrost thaw in Arctic rivers. *Geophysical Research Letters*, *42*(8), 2830–2835. https://doi.org/10.1002/2015gl063498

Spencer, R. G., Stubbins, A., Hernes, P. J., Baker, A., Mopper, K., Aufdenkampe, A. K., et al. (2009). Photochemical degradation of dissolved organic matter and dissolved lignin phenols from the Congo River. *Journal of Geophysical Research: Biogeosciences*, *114*(G3). https://doi.org/10.1029/2009jg000968

Spencer, R. G., Vermilyea, A., Fellman, J., Raymond, P., Stubbins, A., Scott, D., & Hood, E. (2014). Seasonal variability of organic matter composition in an Alaskan glacier outflow: Insights into glacier carbon sources. *Environmental Research Letters*, *9*(5), 055005. https://doi.org/10.1088/1748-9326/9/5/055005

Stibal, M., Hasan, F., Wadham, J. L., Sharp, M. J., & Anesio, A. M. (2012). Prokaryotic diversity in sediments beneath two polar glaciers with contrasting organic carbon substrates. *Extremophiles*, *16*(2), 255–265. https://doi.org/10.1007/s00792-011-0426-8

Stibal, M., Šabacká, M., & Žárský, J. (2012). Biological processes on glacier and ice sheet surfaces. *Nature Geoscience*, *5*(11), 771. https://doi.org/10.1038/ngeo1611

Stubbins, A., & Dittmar, T. (2015). Illuminating the deep: Molecular signatures of photochemical alteration of dissolved organic matter from North Atlantic Deep Water. *Marine Chemistry*, *177*, 318–324. https://doi.org/10.1016/j.marchem.2015.06.020

Stubbins, A., Hood, E., Raymond, P. A., Aiken, G. R., Sleighter, R. L., Hernes, P. J., et al. (2012). Anthropogenic aerosols as a source of ancient dissolved organic matter in glaciers. *Nature Geoscience*, *5*(3), 198. https://doi.org/10.1038/ngeo1403

Stubbins, A., Hubbard, V., Uher, G., Law, C. S., Upstill-Goddard, R. C., Aiken, G. R., & Mopper, K. (2008). Relating carbon monoxide photoproduction to dissolved organic matter functionality. *Environmental Science & Technology*, *42*(9), 3271–3276. https://doi.org/10.1021/es703014q

Stubbins, A., Niggemann, J., Dittmar, T., & Herndl, G. (2012). Photo-lability of deep ocean dissolved black carbon. *Biogeosciences*, *9*(5). https://doi.org/10.5194/bg-9-1661-2012

Stubbins, A., Spencer, R. G., Chen, H., Hatcher, P. G., Mopper, K., Hernes, P. J., et al. (2010). Illuminated darkness: Molecular signatures of Congo River dissolved organic matter and its photochemical alteration as revealed by ultrahigh precision mass spectrometry. *Limnology & Oceanography*, *55*(4), 1467–1477. https://doi.org/10.4319/lo.2010.55.4.1467

Wadham, J., Bottrell, S., Tranter, M., & Raiswell, R. (2004). Stable isotope evidence for microbial sulphate reduction at the bed of a polythermal high Arctic glacier. *Earth and Planetary Science Letters*, *219*(3–4), 341–355. https://doi.org/10.1016/s0012-821x(03)00683-6

Waggoner, D. C., Chen, H., Willoughby, A. S., & Hatcher, P. G. (2015). Formation of black carbon-like and alicyclic aliphatic compounds by hydroxyl radical initiated degradation of lignin. *Organic Geochemistry*, *82*, 69–76. https://doi.org/10.1016/j.orggeochem.2015.02.007

Waggoner, D. C., Wozniak, A. S., Cory, R. M., & Hatcher, P. G. (2017). The role of reactive oxygen species in the degradation of lignin derived dissolved organic matter. *Geochimica et Cosmochimica Acta*, *208*, 171–184. https://doi.org/10.1016/j.gca.2017.03.036

Wagner, S., Ding, Y., & Jaffé, R. (2017). A new perspective on the apparent solubility of dissolved black carbon. *Frontiers of Earth Science*, *5*, 75. https://doi.org/10.3389/feart.2017.00075

Wozniak, A., Willoughby, A., Gurganus, S., & Hatcher, P. G. (2014). Distinguishing molecular characteristics of aerosol water soluble organic matter from the 2011 trans-North Atlantic US GEOTRACES cruise. *Atmospheric Chemistry and Physics*, *14*(16). https://doi.org/10.5194/acp-14-8419-2014

Wozniak, A. S., Bauer, J. E., Sleighter, R. L., Dickhut, R. M., & Hatcher, P. (2008). Molecular characterization of aerosol-derived water soluble organic carbon using ultrahigh resolution electrospray ionization Fourier transform ion cyclotron resonance mass spectrometry. *Atmospheric Chemistry and Physics*, *8*(17). https://doi.org/10.5194/acp-8-5099-2008

Wozniak, A. S., Goranov, A. I., Mitra, S., Bostick, K. W., Zimmerman, A. R., Schlesinger, D. R., et al. (2020). Molecular heterogeneity in pyrogenic dissolved organic matter from a thermal series of oak and grass chars. *Organic Geochemistry*, *148*, 104065. https://doi.org/10.1016/j.orggeochem.2020.104065

Zhou, L., Zhou, Y., Hu, Y., Cai, J., Liu, X., Bai, C., et al. (2019). Microbial production and consumption of dissolved organic matter in glacial ecosystems on the Tibetan Plateau. *Water Research*, *160*, 18–28. https://doi.org/10.1016/j.watres.2019.05.048

Zhou, Y., Zhou, L., He, X., Jang, K.-S., Yao, X., Hu, Y., et al. (2019). Variability in dissolved organic matter composition and biolability across gradients of glacial coverage and distance from glacial terminus on the Tibetan Plateau. *Environmental Science & Technology*, *53*(21), 12207–12217. https://doi.org/10.1021/acs.est.9b03348

Zito, P., Podgorski, D. C., Johnson, J., Chen, H., Rodgers, R. P., Guillemette, F., et al. (2019). Molecular-level composition and acute toxicity of photosolubilized petrogenic carbon. *Environmental Science & Technology*, *53*(14), 8235–8243. https://doi.org/10.1021/acs.est.9b01894